Nanomaterials and Nanotechnology

OPEN ACCESS
ARTICLE

Preparation of Iron-nickel Alloy Nanostructures via Two Cationic Pyridinium Derivatives as Soft Templates

Regular Paper

Jingxin Zhou[1], Tifeng Jiao[1,2,3]*, Wenfeng Guo[1], Bo Wang[1], Haiying Guo[1], Linfan Cui[1], Qingrui Zhang[1]*, Yan Chen[1] and Qiuming Peng[2]

1 Hebei Key Laboratory of Applied Chemistry, School of Environmental and Chemical Engineering, Yanshan University, Qinhuangdao, P. R. China
2 State Key Laboratory of Metastable Materials Science & Technology, Yanshan University, Qinhuangdao, P. R. China
3 National Key Laboratory of Biochemical Engineering, Institute of Process Engineering, Chinese Academy of Sciences, Beijing, P. R. China
*Corresponding author(s) E-mail: tfjiao@ysu.edu.cn; zhangqr@ysu.edu.cn

Received 05 February 2015; Accepted 18 August 2015

DOI: 10.5772/61296

Abstract

In this paper, crystalline iron-nickel alloy nanostructures were successfully prepared from two cationic pyridinium derivatives as soft templates in solution. The crystal structure and micrograph of FeNi alloy nanostructures were characterized by X-ray diffraction, scanning electron microscopy and transmission electron microscopy, and the content was confirmed by energy-dispersive spectrometry. The results indicated that the as-prepared nanostructures showed slightly different diameter ranges with the change of cationic pyridinium derivatives on the surface. The experimental data indicated that the adsorption of cationic pyridinium compounds on the surface of particles reduces the surface charge, leading to an isotropic distribution of the residual surface charges. The magnetic behaviours of as-prepared FeNi alloy nanostructures exhibited disparate behaviours, which could be attributed to their grain sizes and distinctive structures. The present work may give some insight into the synthesis and character of new alloy nanomaterials with special nanostructures using new soft templates.

Keywords nanostructures, iron-nickel alloy, pyridinium derivative, soft template, characterization, self-assembly

1. Introduction

Over the last few decades, the preparation of nanostructures has been attracting considerable attention because of their novel properties of surface effect, small size effect, quantum effect and macro-quantum tunnel effect [1-3]. Nanostructures, especially hierarchical ferromagnetic nanoparticles, are potentially interesting materials due to their fundamental importance and potential applications in fields such as sensors, nano-devices, magnetic recording materials, magnetic logic, high-density magnetic random access memory, biological transportation, etc. [4-10]. In order to obtain well-defined nanoparticle assemblies, various techniques have been developed, such as vapour-based growth techniques, the arc process, the supercritical fluid method, the self-assembly route, the sol-gel method, electrodeposition, hydrothermal synthesis, chemical

vapour deposition, atomic layer deposition and chemical reduction [11-17]. Among these techniques, the template-based self-assembly method is widely adopted not only because it has preferable insulativity, and chemical and heat stability, but also because it is convenient, versatile and inexpensive [18-20].

In addition, FeNi alloy, which is usually called permalloy, shows a series of physical characteristics with the variation of ratios [21-23], and it has superparamagnetic properties and the high chemical stability needed in biotechnology and separation. Until now, the nanostructures of FeNi alloy have been investigated widely [24-25]. However, the comparative study of the fabrication process, which is important for its magnetic properties, has not been discussed intensively. Jia et al. presented a microwave-assisted route to obtain $FeNi_3$ alloyed nanochains [26]. Zhang et al. successfully fabricated FeNi alloy nanowires and nanotubes in an anodic aluminium oxide template by electrodeposition [27]. Lu et al. demonstrated the synthesis of $FeNi_3$ nanoparticles via a hydrazine reduction method without using any surfactant agent [28]. Interestingly, they have recently reported a simple cetyltrimethylammonium bromide (CTAB)-mediated directed-assembly method for the synthesis of magnetic iron-nickel nanochains in an aqueous solution [29].

Herein, we have designed and prepared $FeNi_3$ nanostructures via two cationic pyridinium derivatives as templates and stabilizers. In the molecular structures of both compounds, the hydrophobic alkyl chains were symmetrically/asymmetrically linked to a pyridine ring as a headgroup to show different molecular skeletons and charge dispersion. The morphology, composition and magnetic properties of the as-prepared FeNi alloy nanostructures are investigated in detail.

2. Experiment

2.1 Materials

The starting materials, 1-bromohexadecane and 4, 4'-dipyridyl, were purchased from Alfa Aesar (Beijing, China) and Sigma-Aldrich (Shanghai, China) Chemicals. Cetylpyridinium bromide (abbreviated as C16Py) with analysis purity was purchased from Sinopharm Chemical Reagent Beijing Co., Ltd, China. The solvents were obtained from Beijing Chemicals and were distilled before use. All other chemical reagents used in this experiment were of analytical grade and used without further purification. Deionized water was used in all cases. 1, 1'-Dihexadecyl-4, 4'-bipyridinium bromide (abbreviated as BiPy) was synthesized by reacting 4, 4'-dipyridyl with 1-bromohexadecane according to a previous report [30]. Put simply, the 1-bromohexadecane and 4, 4'-dipyridyl were heated in dried ethanol for two days at 78 °C. After that, the reaction mixtures were cooled and evaporated to dryness. Then, the residues were purified by recrystallization in ethanol solution as a yellow solid. The final product was confirmed by ^1H NMR and elemental analysis. The molecular structures of both compounds with pyridinium headgroups are shown in Fig. 1 (C16Py and BiPy).

2.2 Nanostructures' Preparation

Iron-nickel alloy nanostructures were prepared by reduction of Fe^{2+} and Ni^{2+} in an aqueous solution using C16Py and BiPy as surfactant agents, respectively. In a typical process, similar to that of a previous report [28], $NiCl_2$ $6H_2O$ (30 mmol) and $FeCl_2$ $4H_2O$ (10 mmol) were homogeneously dissolved in 200 mL of distilled water. After undergoing magnetic stirring for 10 min at room temperature, sodium hydroxide (NaOH, 1M) solution was added drop-wise to the above solution to adjust the pH value in the range $10 \le pH \le 13$. Afterwards, 0.16 mol (four times in excess of metal ions) aqueous hydrazine (N_2H_4 H_2O, 80% concentration) and 2-20 mL (0.1 mM) C16Py or BiPy solution were added to the solution as reducing agent and stabilizer agent, respectively. This reduction reaction was allowed to proceed for 12 h. The final products were collected and washed with deionized water and ethanol several times. Finally, the precipitates were dried in a vacuum oven at 40 °C.

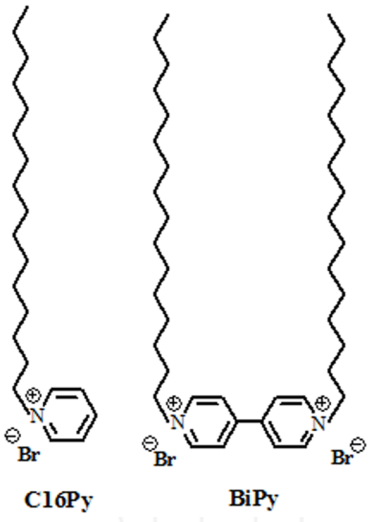

Figure 1. Molecular structures and abbreviations of two cationic pyridinium derivatives

2.3 Characterization

Scanning electron microscope (SEM) pictures were taken using a Hitachi S-4800 field emission scanning electron microscope (Chiyoda-ku, Japan) with the accelerating voltage of 5-15 kV. The chemical compositions of the as-made powders were analysed by energy-dispersive X-ray spectroscopy (EDXS) equipped on the SEM. All transmission electron microscope (TEM) measurements were carried out using HT7700 equipment (Hitachi, Tokyo, Japan). Single drops of the samples were used to slightly coat 300 mesh copper grids covered with thin amorphous carbon films for analysis. Atomic force microscope (AFM)

images were recorded using a Nanoscope VIII Multimode Scanning Probe Microscope (Veeco Instrument, Plainview, NY, USA) with silicon cantilever probes. The X-ray diffraction (XRD) measurement was conducted using a Rigaku D/max 2550PC diffractometer (Rigaku Inc., Tokyo, Japan). The XRD pattern was obtained using CuKα radiation with an incident wavelength of 0.1542 nm under a voltage of 40 kV and a current of 200 mA. The scan rate was 0.5° min^{-1}. Transmission Fourier transform infrared (FT-IR) spectra were obtained using a Nicolet iS10 FT-IR spectrophotometer from Thermo Fisher Scientific Inc. (Waltham, MA, USA) with an average of 16 scans and at a resolution of 4 cm^{-1}. The magnetic properties of the samples were tested using a vibrating sample magnetometer (VSM) from the Physical Property Measurement System (PPMS, Quantum design Model 6000). The powders were aligned under a 10 kOe field and solidified with epoxy resin for the VSM measurements.

3. Results and Discussion

To obtain a visual insight into the as-prepared iron-nickel nanostructures, their typical morphologies were first studied via the SEM technique, as shown in Fig. 2. A general overview of SEM images shows that these products are composed of many nanoparticles with a rough surface and different diameter ranges. From the particle-size distribution histograms of iron-nickel nanoparticles, it can be clearly observed that the size distributions of nanostructures of the two pyridinium derivatives are different. The size distribution of nanostructures from C16Py (0.1 mM, 2 mL) is about 80-140 nm. As for the case of BiPy under the same conditions, the main ranges changed to 100-160 nm. In addition, the typical EDXS of the as-prepared nanostructure originating from C16Py showed obvious Fe and Ni peaks. From the peak intensity, the atomic percentage of Ni is measured as 75.33% of the sum of Fe and Ni atoms, close to the theoretical value of the content of the precursor. This proves that Ni(II) and Fe(II) salts are almost reduced to zerovalent metals. A similar curve was obtained for nanoparticles from BiPy used as a template. In addition, the appearance of a weak Br element peak at 1.5 keV is mainly attributed to the absorption capacity on particle surface of cationic pyridinium derivatives C16Py and BiPy as templates on the particles' surface. At the same time, the C and N elements are not readable due to the trace amounts on the surface and the shielding of light elements. In addition, representative AFM images (Fig. 3) from a 2D perspective with section analysis and from a 3D perspective with depth histogram of the iron-nickel nanostructure originating from C16Py clearly show that the maximum diameter of the nanoparticles is around 117 nm, which well accords with the SEM data above. Furthermore, the TEM images in Fig. 4 also confirmed that the synthesized nanomaterials took the structure of a solid sphere with some small protuberances on the interface. The obtained alloy nanoparticles were also gram-scaled and dried in a vacuum oven. During preparation of SEM or TEM samples, just a little powder or a single drop of the samples' solutions were used to slightly coat the conductive tape or copper grid. Therefore, many of the as-prepared particles stacked tightly in the pictures.

Moreover, the experimental data indicated that the effect of concentrations of pyridinium derivatives did not seem sensitive to regulating the prepared morphologies. As cationic pyridinium derivatives, C16Py and BiPy molecules have positively charged pyridinium headgroups and long hydrophobic alkyl chains. In a colloid dispersion with a high pH value, iron-nickel nanostructures carry negative surface charges in the solution, which create a strong repulsive force inhibiting the aggregation of the particles. At the same time, cationically charged molecules can adsorb on the negatively charged surface of the particles and effectively reduce the overall charge on the surfaces, leading to a reduced repulsive force [31-32]. In the present work, the cationic pyridinium compounds were absorbed on the particle surface of nanostructures to reduce the overall charge, and which were responsible for the formation of small protuberances or wrinkles on the particles' surfaces. It should be noted that at present, the obtained alloy nanoparticles showed uneven surfaces with grey shadows in TEM pictures. The grey shadow may be caused by the aggregation of alkyl chains in stabilizers. In addition, the roughness of the surface can be attributed to the reduced charge and anisotropic aggregation of pyridine rings absorbed on the particle surface.

In addition, with the purpose of investigating the crystal structure and purity of the as-prepared products, the typical XRD patterns of all samples were measured from 2θ angle values of 20-80°. The nanostructures obtained from C16Py at different amounts were taken as an example, as shown in Fig. 5 (A). Though synthesized from pyridinium derivatives of different amounts, the structures of the resulting nanostructures are similar. All the featured XRD peaks can be indexed as a face-centred cubic (FCC) $FeNi_3$ alloy, consistent with the standard card (JCPDS card no. 38-0419, space group Pm3m (221); cell parameter $\alpha = 0.3545$ nm). When compared with standard patterns, the nanostructures presented the (111) preferred orientation characteristics [27, 29]. No XRD peaks for Fe and (FCC)-Ni can be observed. In addition, no impurity phases such as iron-nickel oxides and hydroxides were detected. Similar XRD curves were obtained for nanoparticles from BiPy as a template.

We also measured the FT-IR spectra of as-prepared nanostructures to investigate the possible functional groups on the particles' surfaces. For the spectra of nanostructures from C16Py in Fig. 5 (B), some characteristic peaks were observed at 3423, 2919, 2850, 1623, 1455 and 1383 cm^{-1}. These bands can be assigned to the O-H stretching, alkyl chain stretching, stretching of the pyridine ring, scissoring of alkyl chain and O-H, respectively [33-34]. With the incremental use of various C16Py amounts in the preparation process, the relative intensities of peaks assigned to alkyl chain stretching were enhanced, suggesting more adsorption of C16Py molecules on the particles' surfaces. Similar tendencies in IR spectra were obtained for

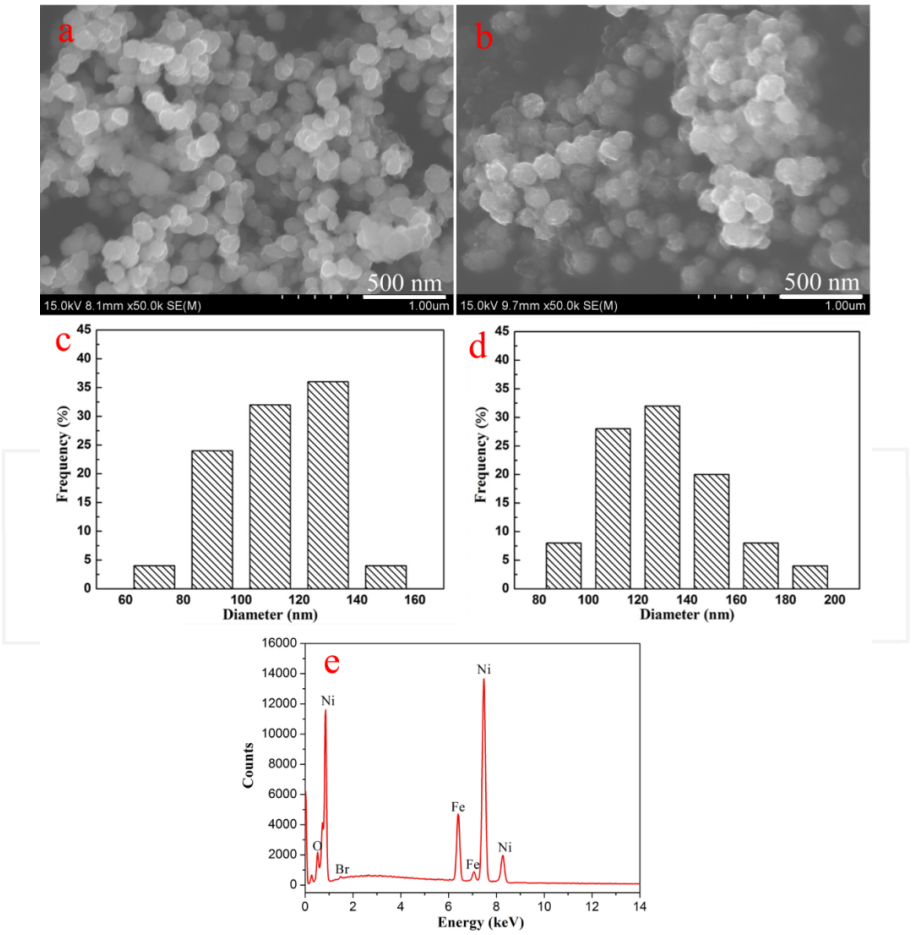

Figure 2. SEM images of obtained iron-nickel nanostructures with a concentration of 0.1 mM and an amount of 2 mL: C16Py (a) and BiPy (b); images (c) and (d) are particle size distribution histograms of iron-nickel nanoparticles from SEM images (a) and (b), respectively; typical EDXS (e) of the nanostructure originated from (a)

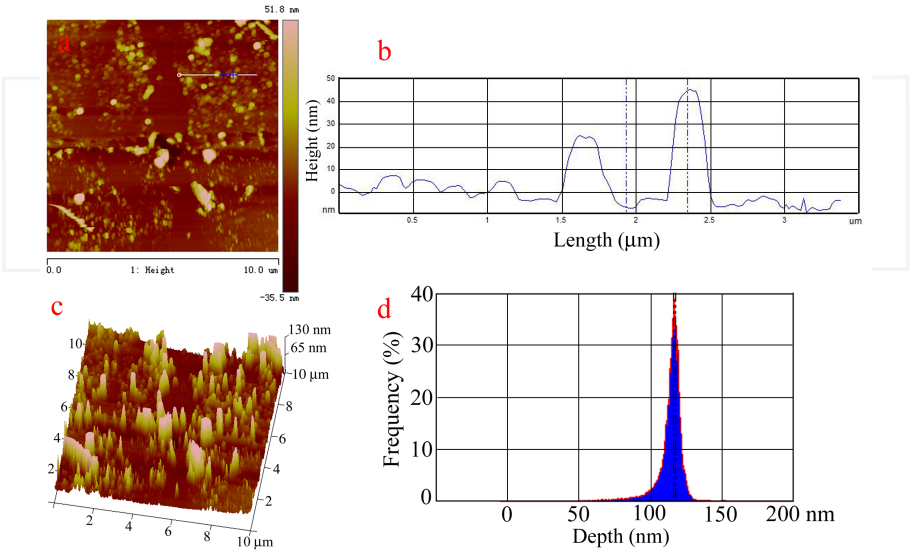

Figure 3. AFM images from a 2D perspective with section analysis and from a 3D perspective with depth histogram of iron-nickel nanostructures originating from C16Py at the amount of 2 mL

nanoparticles using BiPy as the template. The present experimental data verified that the cationic pyridinium derivatives could act as templates and stabilizing agents.

Fig. 6 shows typical photographs of dispersed iron-nickel samples in solution and after using a magnetic field, which demonstrated strong magnetic properties of the prepared

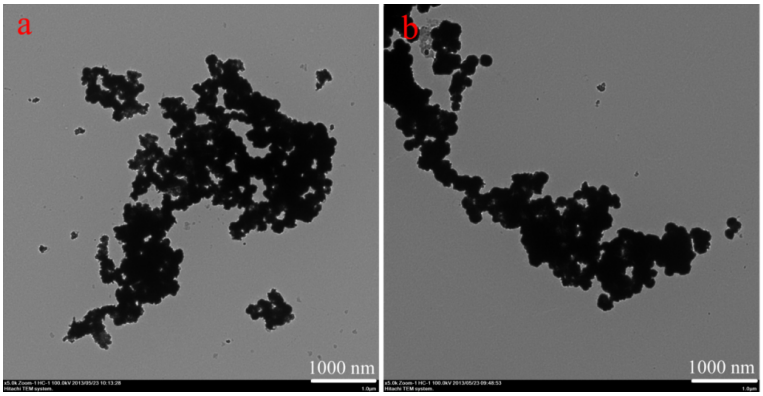

Figure 4. TEM images of obtained iron-nickel nanostructures at a concentration of 0.1 mM and an amount of 2 mL: C16Py (a) and BiPy (b)

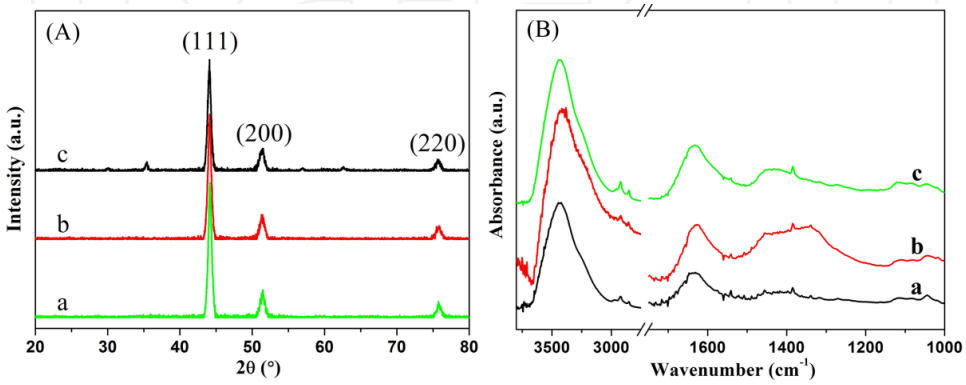

Figure 5. X-ray diffraction patterns (A) and FT-IR spectra (B) of nanostructures obtained from C16Py at a concentration of 0.1 mM and with different amounts: (a) 2 mL, (b) 10 mL and (c) 20 mL

products. Fig. 7 shows magnetic hysteresis curves of the as-synthesized iron-nickel nanostructures carried out at room temperature in an applied magnetic field sweeping from -10 kOe to 10 kOe. For the curves of nanostructures from C16Py, the corresponding saturation magnetization strengths were 81, 84 and 97 emu/g, increasing with incremental amounts of C16Py. In addition, as in the case of samples from BiPy with different amounts, the saturation magnetization strengths showed slight changes, with the values of 81, 79 and 81 emu/g, respectively. All presently obtained values were higher than those of the bulk alloy (76 emu/g) [35-36], mainly due to the much smaller particle sizes and the magnetic interfaces, which suggested more organized stacking of stabilizer agents on particles' surfaces.

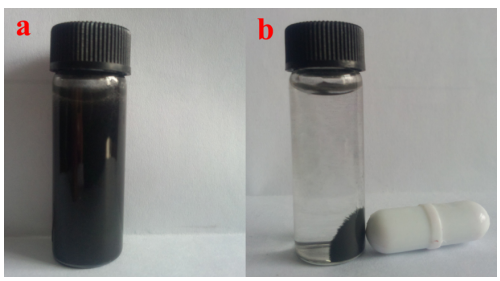

Figure 6. Typical photographs of dispersed nanostructures in solution (a) and after using a magnetic field (b)

Considering the obtained experimental results described above and previous reports, a different process of the preparation of iron-nickel alloy nanostructures via cationic pyridinium derivatives was proposed. As for presently used C16Py and BiPy with pyridine ring as headgroups, in comparison with the single quaternary ammonium compound CTAB, two template molecules demonstrated larger spatial hindrance and better charge dispersion between pyridine rings. Therefore, the prepared iron-nickel nanostructures showed a slightly larger particle diameter with negative surface charges and adsorbed, charged pyridinium headgroups in solution. This leads to an isotropic distribution of the residual surface charges, generating a uniform stacking of nanoparticles. In addition, it is interesting to note that the presently obtained results show obvious differences with those of the relative report of $FeNi_3$ nanoparticles preparation with CTAB as template [29]. In that work, the iron-nickel nanochains were formed by an orderly self-assembly process. The potential applications of the presently prepared nanostructures are currently under investigation in various relative fields of nanomaterials and nanotechnology.

4. Conclusions

In summary, iron-nickel alloy nanostructures with different size ranges have been successfully prepared via cationic pyridinium derivatives used as templates in solution. The

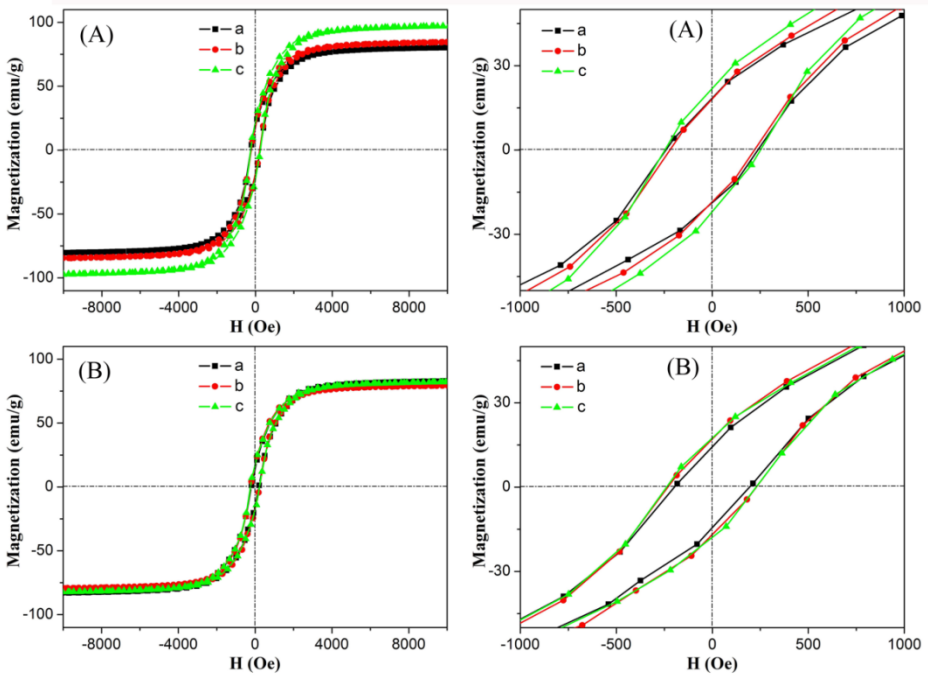

Figure 7. Magnetic hysteresis loops of nanostructures. C16Py (A) and BiPy (B) obtained with different amounts: (a) 2 mL, (b) 10 mL and (c) 20 mL

experimental results showed that the adsorption of cationic pyridinium compounds on the surface of particles reduces the surface charge, leading to an isotropic distribution of the residual surface charges. A significantly changed magnetic coercivity has been observed for the nanostructures compared to the bulk permalloy. The prepared nanostructures and magnetic properties have many potential applications in nanoscience and material fields due to their scientific values.

5. Acknowledgements

This work was financially supported by the National Natural Science Foundation of China (Nos. 21473153 and 21207112), the Natural Science Foundation of Hebei Province (No. B2013203108), Science Foundation for the Excellent Youth Scholars from Universities and Colleges of Hebei Province (No. YQ2013026), Support Program for the Top Young Talents of Hebei Province, the Scientific and Technological Research and Development Program of Qinhuangdao City (No. 201502A006), and the Open Foundation of National Key Laboratory of Biochemical Engineering (Institute of Process Engineering, Chinese Academy of Sciences).

6. References

[1] Xia Y N, Yang P D, Sun Y G, Wu Y Y, Mayers B, Gates B, Yin Y D, Kim F, Yan H Q (2003) One-dimensional nanostructures: synthesis, characterization, and applications. Adv. Mater. 5: 353-389.

[2] Bai C, Liu M (2013) From chemistry to nanoscience: not just a matter of size. Angew. Chem. Int. Ed. 52: 2678-2683.

[3] Li W Q, Xiao X H, Stepanov A L, Dai Z G, Wu W, Cai G X, Ren F, Jiang C Z (2013) The ion implantation-induced properties of one-dimensional nanomaterials. Nanoscale Res. Lett. 8: 175.

[4] Li Y L, Tang S L, Xie R, Wang Y, Yang M, Gao J L, Xia W B, Du Y W (2012) Fabrication and magnetic properties of free-standing Ni nanotube arrays with controllable wall thickness. Appl. Phys. Lett. 100: 052402.

[5] La Flamme K E, Popat K C, Leoni L, Markiewicz E, La Tempa T J, Roman B B, Grimes C A, Desai T A: Biocompatibility of nanoporous alumina membranes for immunoisolation. Biomaterials 28: 2638-2645.

[6] Salem A K, Searson P C, Leong K W (2003) Multifunctional nanorods for gene delivery. Nature Mater. 2: 668-671.

[7] Davis D, Zamanpour M, Moldovan M, Young D, Podlaha E J (2010) Electrodeposited, GMR CoNiFe-Cu nanowires and nanotubes from electrolytes maintained at different temperatures. J. Electrochem. Soc. 157: 317-322.

[8] Chen J Y, Ahmad N, Shi D W, Zhou W P, Han X F (2011) Synthesis and magnetic characterization of Co-NiO-Ni core-shell nanotube arrays. J. Appl. Phys. 110: 073912.

[9] Zhang X Y, Wen G H, Chan Y F, Zheng R K, Zhang X X, Wang N (2003) Fabrication and magnetic properties of ultrathin Fe nanowire arrays. Appl. Phys. Lett. 83: 3341-3343.

[10] Wang X W, Yuan Z H, Fang B C (2011) Template-based synthesis and magnetic properties of Ni

nanotube arrays with different diameters. Mater. Chem. Phys. 125: 1-4.

[11] Huczko A (2000) Template-based synthesis of nanomaterials. Appl. Phys. A 70: 365-376.

[12] Han X F, Shamaila S, Sharif R, Chen J Y, Liu H R, Liu D P (2009) Structural and magnetic properties of various ferromagnetic nanotubes. Adv. Mater. 21: 4619-4624.

[13] Escrig J, Bachmann J, Jing J, Daub M, Altbir D, Nielsch K (2008) Crossover between two different magnetization reversal modes in arrays of iron oxide nanotubes. Phys. Rev. B 77: 214421.

[14] Li F S, Zhou D, Wang T, Wang Y, Song L J, Xu C T (2007) Fabrication and magnetic properties of FeCo alloy nanotube array. J. Appl. Phys. 101: 014309.

[15] Hernàndez-Vélez M (2006) Nanowires and 1D arrays fabrication: an overview. Thin Solid Films 495: 51-63.

[16] Sellmyer D J, Zheng M, Skomski R (2001) Magnetism of Fe, Co and Ni nanowires in self-assembled arrays. J. Phys: Condens. Matter. 13: 433-460.

[17] Li G, Guo Y, Sun X, Wang T, Zhou J, He J (2012) Synthesis and microwave absorbing properties of FeNi alloy incorporated ordered mesoporous carbon-silica nanocomposite. J. Phys. Chem. Solids 73: 1268-1273.

[18] Harraz F A (2013) Synthesis and surface properties of magnetite (Fe_3O_4) nanoparticles infiltrated into porous silicon template. Appl. Surf. Sci. 287: 203-210.

[19] Nyamjav D, Ivanisevic A (2005) Templates for DNA-templated Fe_3O_4 nanoparticles. Biomaterials 26: 2749-2757.

[20] Bizdoaca E L, Spasova M, Farle M, Hilgendorff M, Caruso F (2002) Magnetically directed self-assembly of submicron spheres with a Fe_3O_4 nanoparticle shell. J. Magn. Magn. Mater. 240: 44-46.

[21] Li H Q, Ebrahimi F (2006) Tensile behavior of a nanocrystalline Ni-Fe alloy. Acta. Mater. 54: 2877-2886.

[22] Leith S D, Ramli S, Schwartz D T (1999) Characterization of NixFe1-x (0.10<x<0.95) electrodeposition from a family of sulfamate-chloride electrolytes. J. Electrochem. Soc. 146: 1431-1435.

[23] Fu X L, Wang Y, Li P G, Chen L M, Zhang H Y, Tu Q Y, Li L H, Tang W H (2005) Large-scale fabrication and magnetic properties of $Ni_{80}Fe_{20}$ nanowire arrays. Acta. Phys. Sin. 54: 1693-1696.

[24] Zhou D, Cai L H, Wen F S, Li F S (2007) Template synthesis and magnetic behavior of FeNi alloy nanotube arrays. Chin. J. Chem. Phys. 20: 821-825.

[25] Khan H R, Petrikowski K (2000) Anisotropic structural and magnetic properties of arrays of $Fe_{26}Ni_{74}$ nanowires electrodeposited in the pores of anodic alumina. J. Magn. Magn. Mater. 215-216: 526-528.

[26] Jia J C, Yu J C, Wang Y X J, Chan K M (2010) Magnetic nanochains of $FeNi_3$ prepared by a template-free microwave-hydrothermal method. ACS Appl. Mater. Inter. 2: 2579-2584.

[27] Zhang X, Zhang H, Wu T, Li Z, Zhang Z, Sun H (2013) Comparative study in fabrication and magnetic properties of FeNi alloy nanowires and nanotubes. J. Magn. Magn. Mater. 331: 162-167.

[28] Lu X G, Liang G Y, Zhang Y M (2007) Synthesis and characterization of magnetic $FeNi_3$ particles obtained by hydrazine reduction in aqueous solution. Mater. Sci. Eng. B-Solid 139: 124-127.

[29] Lu X, Liu Q, Huo G, Liang G, Sun Q, Song X (2012) CTAB-mediated synthesis of iron-nickel alloy nanochains and their magnetic properties. Colloid Surf. A-Physicochem. Eng. Asp. 407: 23-28.

[30] Zhang L, Jiao T, Shao X, Li Z, Liu M (2006) The effect of charge distributing in head group on the supramolecular chirality of complex film between achiral TPPS with amphiphiles. Colloid Surf. A-Physicochem. Eng. Asp. 284-285: 130-134.

[31] Atkin R, Craig V S J, Wanless E J, Biggs S (2003) Mechanism of cationic surfactant adsorption at the solid-aqueous interface. Adv. Colloid Interface Sci. 103: 219-304.

[32] Rutland M W, Parker J L (1994) Surface forces between silica surfaces in cationic surfactant solutions: adsorption and bilayer formation at normal and high pH. Langmuir 10: 1110-1121.

[33] Jiao T F, Wang Y J, Gao F Q, Zhou J X, Gao F M (2012) Photoresponsive organogel and organized nanostructures of cholesterol imide derivatives with azobenzene substituent groups. Prog. Nat. Sci. 22: 64-70.

[34] Jiao T F, Gao F Q, Wang Y J, Zhou J X, Gao F M, Luo X Z (2012) Supramolecular gel and nanostructures of bolaform and trigonal cholesteryl derivatives with different aromatic spacers. Curr. Nanosci. 8: 111-116.

[35] Ammar M, Mazaleyrat F, Bonnet J P, Audebert P, Brosseau A, Wang G, Champion Y (2007) Synthesis and characterization of core-shell structure silica-coated $Fe_{29.5}Ni_{70.5}$ nanoparticles. Nanotechnology 18: 285606.

[36] An Z G, Pan S L, Zhang J J (2009) Synthesis and tunable assembly of spear-like nickel nanocrystallites: from urchin-like particles to prickly chains. J. Phys. Chem. C 113: 1346-1351.